NELF-E RRM Undergoes Major Structural Changes in Flexible Protein Regions on Target RNA Binding[†]

Jampani Nageswara Rao, Kristian Schweimer, Sabine Wenzel, Birgitta M. Wöhrl, and Paul Rösch*

Lehrstuhl Biopolymere and Research Center for Bio-Macromolecules, Universität Bayreuth, 95440 Bayreuth, Germany

Received December 12, 2007; Revised Manuscript Received January 31, 2008

ABSTRACT: The E subunit of the human heterotetrameric negative transcription elongation factor (NELF-E) contains a canonical $\beta\alpha\beta\beta\alpha\beta$ RNA recognition motif (RRM) that binds to a wide variety of RNA sequences. These induce very similar conformational changes in the RRM as determined by nuclear magnetic resonance spectroscopy. Although the RNA binding interface of a canonical RRM is mainly located at its β-sheet surface, for NELF-E RRM large chemical shift perturbations are observed for residues in the flexible C-terminal region and the loop between β_3 and α_2, and both regions are distant from the interface. We determined the solution structure of single-stranded transactivator responsive element (TAR) RNA-bound NELF-E RRM. This structure clearly shows that RNA binding to NELF-E RRM induces formation of a helix in the C-terminus. The RNA-bound form of NELF-E RRM is very similar to the RNA-bound form of U1A RRM, although the C-terminus of the NELF-E RRM is unstructured in the free protein, whereas it is helical in the U1A protein. Thus, RNA binding to NELF-E RRM induces a conformational change toward the U1A structure, resulting in highly similar RNA binding conformations for both proteins.

The RNA recognition motif (RRM),[1] also known as ribonucleoprotein (RNP) domain or RNA binding domain, is one of the most common RNA binding domains, and proteins containing this domain are involved in most steps of eukaryotic gene expression (*1–3*). RRM domains typically consist of 90 amino acids and fold into modules with a $\beta_1\alpha_1\beta_2\beta_3\alpha_2\beta_4$ topology, where the four β-strands form an antiparallel β-sheet (*4*). Whereas one surface of the β-sheet is involved in hydrophobic packing with the two α-helices, the other is the RNA binding surface. RRM domains contain two highly conserved ribonucleoprotein motifs, RNP1 and RNP2, located in the central β-strands. The aromatic amino acids of the RNP motifs are thought to be involved in base-stacking interactions with unpaired RNA bases (*3*). The RRM target RNAs are diverse in sequence and secondary structure. In general, RRMs use loop regions as well as N- and C-terminal extensions along with variations in the β-sheet surface (*5*) to obtain RNA binding specificity, but individual RRMs use different mechanisms for RNA recognition depending on their RNA target.

Negative transcription elongation factor (NELF) is a heterotetrameric protein of four subunits, NELF-A, NELF-B, alternatively spliced NELF-C or NELF-D, and NELF-E (*6*). As a general transcription factor, NELF is involved not only in the regulation of human gene expression (*7, 8*) but also in the regulation of HIV-1 transcription by arresting the elongation complex (*9, 10*). The RNA binding activity of the NELF-E RRM is crucial for the function of NELF, and deletion of NELF-E RRM completely abolishes the function of NELF (*11, 12*). NELF is recruited to the elongation complex by binding to the nascent transcripts of RNA polymerase II (Rpol II) via the NELF-E RRM (*11*). The negative effect of NELF on HIV-1 transcription is counteracted by NELF-E phosphorylation and phosphorylation of the C-terminal domain of Rpol II by positive transcription elongation factor b (p-TEFb) which in turn is recruited to the elongation complex via Zn^{2+}-dependent interaction with HIV-1 transactivator (Tat) protein (*10, 13–15*). NELF-E RRM exhibits a canonical topology, that is, a four-stranded antiparallel β-sheet surface packed against two α-helices, and the N- and the C-termini are unstructured in solution (*16*). Here we explore details of the structural changes induced into the NELF-E RRM upon RNA binding utilizing NMR spectroscopy.

MATERIALS AND METHODS

NMR Spectroscopy. ^{15}N- and ^{13}C,^{15}N-labeled NELF-E RRM was expressed and purified as described (*16*). Synthetic RNA oligonucleotides purified by HPLC were purchased from biomers-GmbH, Ulm, Germany. All NMR experiments were performed at 298 or 303 K on Bruker Avance 700 and Avance 800 spectrometers equipped with cryogenic cooled ^{1}H/^{13}C/^{15}N triple-resonance probes with pulsed-field gradient capabilities. NMR titration experiments were performed on ^{15}N-labeled NELF-E RRM (0.1 mM) by measuring a series of 2D ^{1}H−^{15}N HSQC spectra with addition of unlabeled single-stranded TAR RNA oligonucleotides at various molar ratios, and ^{1}H−^{15}N resonance shift and line width changes

[†] Financial support for this work has been provided by the Deutsche Forschungsgemeinschaft (DFG; Ro617/16-1).

* Corresponding author: phone, +49 921 553540; fax, +49 921 16490459; e-mail, roesch@unibt.de.

[1] Abbreviations: HSQC, heteronuclear single-quantum coherence spectroscopy; NELF-E, negative elongation factor subunit E; RRM, RNA recognition motif; RNP, ribonucleoprotein; TAR, transactivator responsive element; Rpol, RNA polymerase; p-TEFb, positive transcription elongation factor b.

10.1021/bi702429m CCC: $40.75
Published on Web 02/28/2008

were monitored by analysis of these spectra. Normalized chemical shift changes were expressed as the weighted geometric average of ^{1}HN and ^{15}N chemical shift changes for each residue, and normalized chemical shift changes larger than 0.04 ppm were considered significant (*31*).

The dissociation constants K_d were determined from the changes of chemical shifts of ^{15}N-labeled NELF-E RRM observed in a ^{1}H−^{15}N HSQC spectrum after gradual addition of the respective unlabeled binding partners. Changes of chemical shift of signals in the fast-exchange limit were fitted to a two-state model.

$$\delta_{obs} = \delta_P + (\delta_{PL} - \delta_P)\left[\frac{K_D + (1+r)[P]_0}{2[P]_0} - \frac{\sqrt{(K_D + (1+r)[P]_0)^2 - 4[P]_0^2 r}}{2[P]_0}\right] \quad (1)$$

δ_{obs}, δ_P, and δ_{PL} are the chemical shifts for the actual mixture, the free protein, and the completely bound protein, respectively. $[P]_0$ is the total concentration of NELF-E RRM, and r describes the NELF-E RRM/RNA ratio.

To obtain the three-dimensional structure of RNA-bound NELF-E RRM, standard double and triple resonance NMR experiments were recorded. All NMR spectra for the structure determination were recorded at 303 K with a 1:1 complex of 0.5 mM uniformly ^{1}H,^{15}N- and ^{13}C-labeled NELF-E RRM and 0.5 mM unlabeled single-stranded TAR49–57 in buffer containing 10 mM sodium phosphate, pH 6.9, 100 mM NaCl, 1 mM DTT, 10% D_2O, and 0.03% of NaN_3. Distance restraints for structure calculation were derived from three-dimensional ^{13}C- and ^{15}N-edited NOESY-HSQC experiments with mixing times of 120 ms (*36, 37*). NMR data were processed using in-house written software and analyzed with the program package NMRview 5.2.2 (*32*).

Structure Determination. Backbone resonances of NELF-E RRM in complex with TAR49–57 were mainly assigned by following the resonances during the titration. Except for the resonances involved in RNA binding, all resonances could be assigned directly since they did not show any chemical shift perturbations. The resonances exhibiting large chemical shift changes were assigned by observing the characteristic NOEs in ^{15}N NOESY-HSQC spectra. Many protein resonances in the complex gave chemical shifts and patterns of NOE cross-peaks similar to those observed for the free protein. Thus, most of the resonances were assigned by comparing the constant time ^{1}H−^{13}C HSQC spectra of the free and RNA-bound NELF-E RRM. Side chain resonance assignments for residues involved in RNA binding were achieved by following the trace of side chain protons in 3D HCCH-TOCSY and identifying characteristic NOEs in ^{13}C NOESY-HSQC spectra. NOE cross-peaks identified in the 3D ^{15}N and ^{13}C NOESY-HSQC spectra in an iterative procedure as well as hydrogen bonds and $^{3}J_{HNH}$ scalar coupling constants were converted into distance and backbone torsion angle restraints, respectively, as described (*16, 33*). In total, 1929 distance restraints, 32 dihedral angles, and 24 hydrogen bonds were used for the structure calculation (Supporting Information, Table 1). All structure calculations were performed with the program X-PLOR 3.8.5.1 using the three-step simulated annealing protocol (*33, 34*) with floating assignment of prochiral groups (*35*) as described (*16*). The structural coordinates were deposited in the Protein Data Bank (PDB accession code 2jx2).

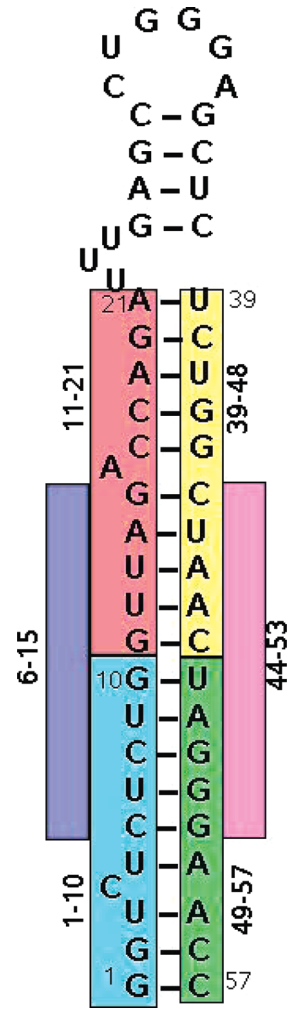

FIGURE 1: Secondary structure of HIV-1 TAR RNA. Sequences of RNA oligonucleotides used for the binding studies with NELF-E RRM are shown in different colors.

RESULTS AND DISCUSSION

RNA Binding Studies. To understand the RNA recognition process by NELF-E RRM in detail and to study the general features of RNA recognition by this protein motif, we performed NELF-E RRM-RNA binding studies by NMR using various single-stranded RNA oligonucleotides derived from the stem region of HIV-1 TAR RNA (Figure 1). Amide proton chemical shifts are usually a very sensitive probe to study side chain perturbations by direct ligand interaction or by protein conformational changes on ligand binding. Addition of unlabeled TAR1–10 to ^{15}N-labeled NELF-E RRM led to chemical shift changes in the ^{1}H−^{15}N HSQC spectra for the residues located in the β-sheet surface of NELF-E RRM (Figure 2), most remarkably for L42, V44, C75, and V78 in the central β-strands but also for E81, K82, and M83 in the loop between β3 and β2 as well as M113, L114, D115, A116, and A117 in the C-terminus. Unambiguous assignment of the amide and nitrogen resonances was facilitated as all resonances were in the fast-exchange regime on the NMR time scale and thus could be traced easily during titration. Although NELF-E RRM binds to all TAR RNA oligonucleotides used in this study, binding resulted in

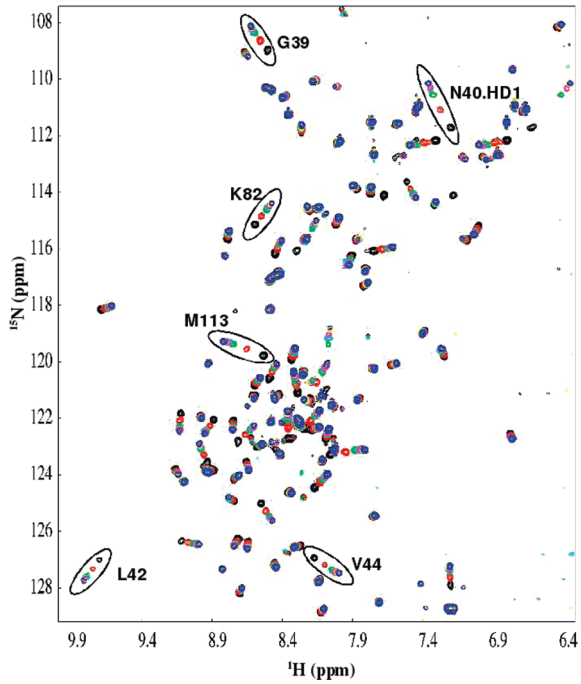

FIGURE 2: Titration of NELF-E RRM with TAR1–10. Overlay of ^{1}H−^{15}N HSQC spectra recorded during the titration with different RNA/protein ratios. Key: black, 0.0; red, 0.25; green, 0.5; cyan, 0.75; magenta, 1.0; yellow, 2.0; blue, 3.0. Those amide resonances showing the strongest chemical shift changes are indicated.

different dynamics of the system as evidenced by different chemical exchange kinetics (Figure 3).

Normalized Chemical Shift Changes. In all titration experiments, regardless of the RNA oligomer added, the same set of amide resonances showed chemical shift perturbations, although with different magnitude. This clearly points to a general structural rearrangement of the NELF-E RRM on RNA binding, independent of the specific sequence of the oligomer. In particular, backbone amide protons and nitrogens located in the β-strands, the loop between β_3 and α_2, and the C-terminal region were strongly influenced, e.g., 0.185 and 0.308 ppm in V44 in the TAR1–10 and the TAR49–57 complexes, respectively. TAR11–21 and TAR49–57 induced the largest chemical shift changes, and the final chemical shift changes in the TAR44–53 could not be detected due to severe resonance broadening. Titration of ^{15}N-labeled NELF-E RRM with TAR1–10, TAR6–15, and TAR39–48 allowed the observation of chemical shift changes for resonances under fast-exchange conditions for amino acids located in the RNA binding region of NELF-E RRM. From these data, K_d values of 21 μM, 35 mM, and 55 μM could be determined (Supporting Information). Thus, NELF-E RRM binds to all RNA oligonucleotides studied in similar fashion with K_ds in the micromolar range, but it does so with differences in detail. The ability of NELF-E RRM to bind a wide variety of single-stranded RNAs, albeit with different affinities, is not surprising, since NELF is involved in regulation of the expression of a wide variety of genes, and the nascent transcripts of Rpol II differ widely in their sequences (*11*).

Mapping of RNA Binding Interface. The RNA binding surface of NELF-E RRM as obtained by chemical shift mapping reveals subtle differences as compared to binding interfaces of other RRMs (*5, 17*−*19*) (Figures 4 and 5). Like other RRMs, NELF-E RRM uses the β-sheet surface and

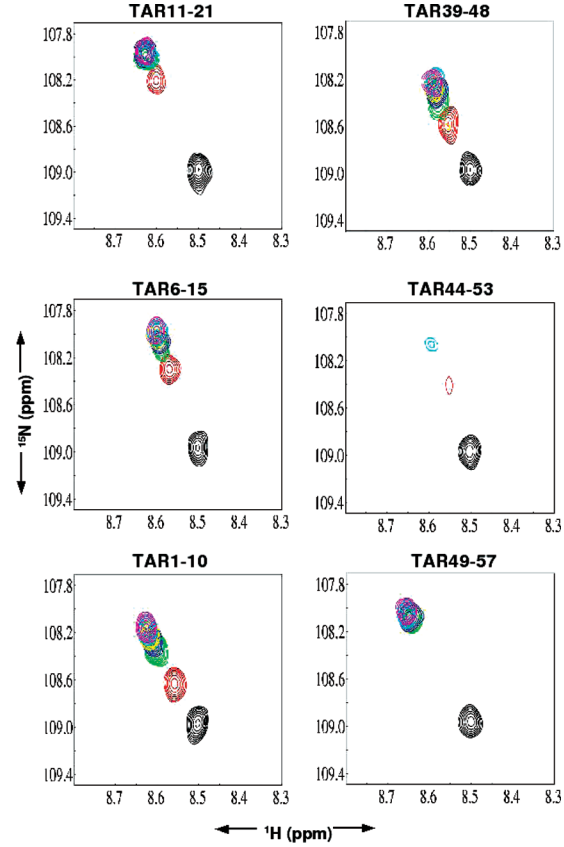

FIGURE 3: Interaction of NELF-E RRM with single-stranded TAR RNA oligonucleotides. Overlays of the G39 amide cross-peak in ^{1}H−^{15}N HSQC spectra at each titration step are shown in different colors. The color codes and RNA/protein ratios are as in Figure 2.

the highly conserved RNP1 and RNP2 motifs to provide a platform for RNA recognition. Usually, if only a single RRM domain is present in a protein, this RRM uses loop regions to provide additional RNA contacts (*20–22*). In the U1A RRM snRNA complex, for example, loop 3 forms an extensive hydrogen bond network and provides hydrophobic contacts with RNA. NELF-E RRM, however, does not show any significant chemical shift perturbation in the loop 3 region upon addition of RNA. Thus, the detailed mode of RNA binding of NELF-E RRM is clearly different than the mode of RNA binding of the U1A RRM.

Addition of RNA to NELF-E RRM results in remarkable chemical shift changes for the resonances located in the N-terminal part of α_2 and the loop between β_2 and β_3. The side chain resonances of N40, located close to this loop, show a significant chemical shift change after RNA addition, although the N40 side chain is located opposite to the RNA binding β-sheet surface, indicating conformational changes in regions of NELF-E RRM that are not directly involved in RNA binding. The same is true for the N-terminal part of α_2; i.e., the amino acid side chains are not close to the binding surface but are still perturbed on RNA binding.

Structure of RNA-Bound NELF-E RRM. Titration of NELF-E RRM with TAR49–57 induced the largest chemical shift changes in the protein and was thus studied more closely. All distance restraints observed for free NELF-E RRM (*16*) were also found in the TAR49–57 complex, indicating that the structures of free and bound protein were highly similar for amino acids 39–107. Forty additional

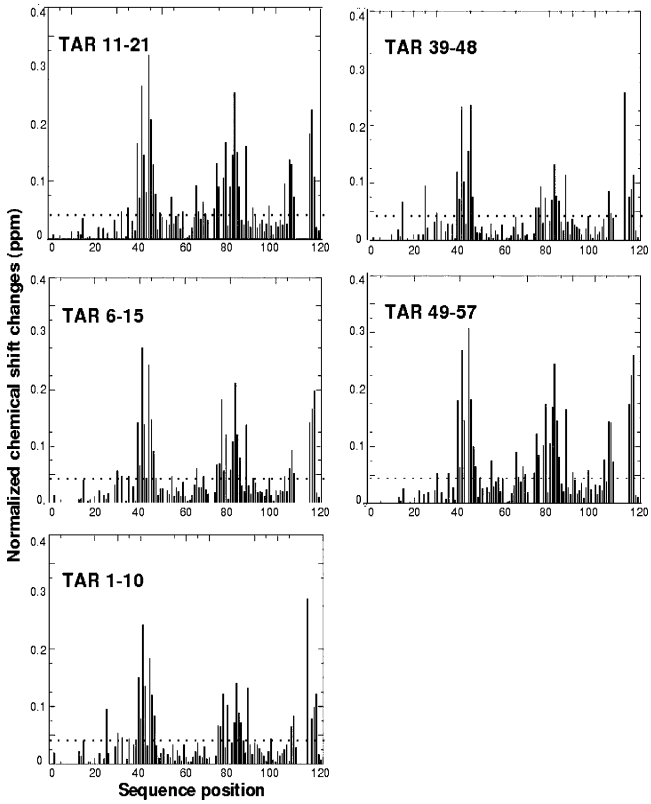

FIGURE 4: Normalized weighted chemical shift changes for NELF-E RRM upon binding to RNA oligonucleotides. Normalized chemical shift changes larger than 0.04 ppm are indicated by a dashed line.

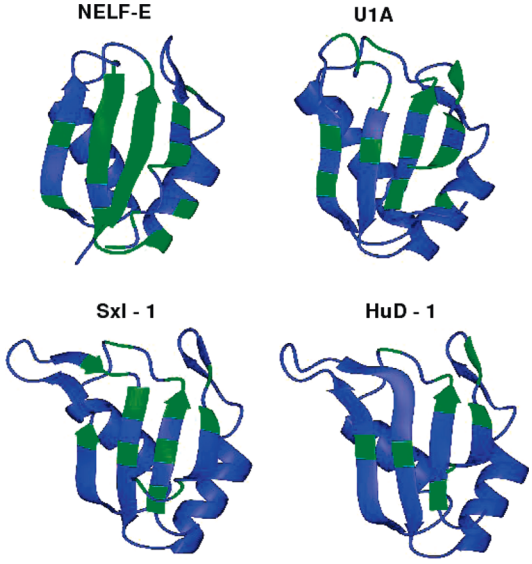

FIGURE 5: Mapping of RNA binding interface. Ribbon representation of RRMs whose structures [NELF-E (2bz2), U1A (1urn), SxI (1b7f), HuD (1fxl)] in the complex with RNA are known. Residues involved in RNA binding are highlighted in green. For NELF-E RRM the amide chemical shift perturbations (those residues showed normalized chemical shifts larger than 0.04 ppm upon binding to TAR49–57) were used to map the RNA binding interface.

interresidual NOEs were observed for NELF-E RRM in the complex, these additional NOEs being mostly from resonances in the C-terminal and the $\beta_3-\alpha_2$ loop regions. Also, significant changes were observed in the NOE pattern of M83 and Q111 on RNA binding, the bound protein showing strong NOEs (0.3 Å) between the γ-protons of M83, Q111 and the

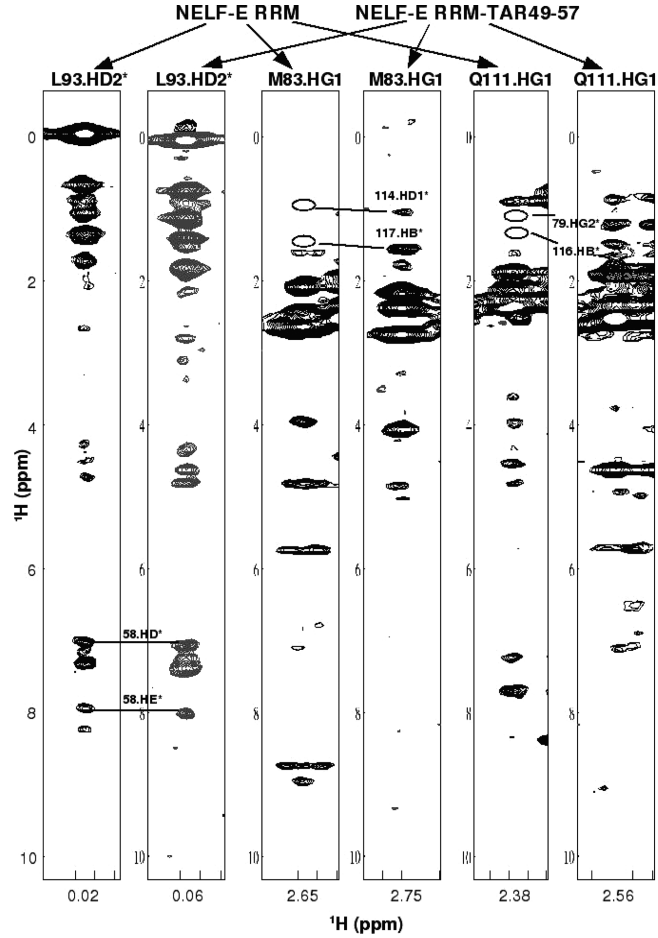

FIGURE 6: Comparison of ^{13}C NOESY-HSQC spectra of free and RNA-bound NELF-E RRM. Interresidual NOEs observed between the C-terminus and around the $\beta3-\alpha2$ loop region are labeled in the NOESY slices of the NELF-E RRM−TAR49–57 complex. The corresponding NOEs not present in the NOESY spectra of free NELF-E RRM are indicated by open circles.

methyl group protons of A117, T79 (Figure 6), indicating a conformational change of the C-terminus of the NELF-E RRM upon binding to TAR49–57.

The final structure calculation resulted in an ensemble of 20 structures showing no distance restraint violation larger than 0.2 Å, no violation of a dihedral angle restraint larger than 3°, and only small deviations from the idealized covalent bond geometry. As expected, the overall global fold of NELF-E RRM remains intact in the complex (Figure 7). The C-terminus of NELF-E RRM, however, is undergoing a major conformational change. Whereas it is highly flexible in the free state, it is stabilized by numerous hydrophobic contacts (I65, T79, M83, M113, L114, A116, A117, and T118) in the RNA-bound conformation, forming a short 3_{10} helix from M113 to D115, close to the $\beta_3-\alpha_2$ loop. This structure formation correlates perfectly well with the large chemical shift changes observed in this region on RNA binding. The C-terminus of NELF-E RRM is located close to the highly conserved aromatic amino acids in the RNP motif and is thus likely involved in RNA binding (Figure 7c), and the basic residues located C-terminally to β_4 (R109, K110) could be involved in electrostatic interaction with the phosphate backbone of the RNA. These structural rearrangements involving the C-terminus reinforces the concept of

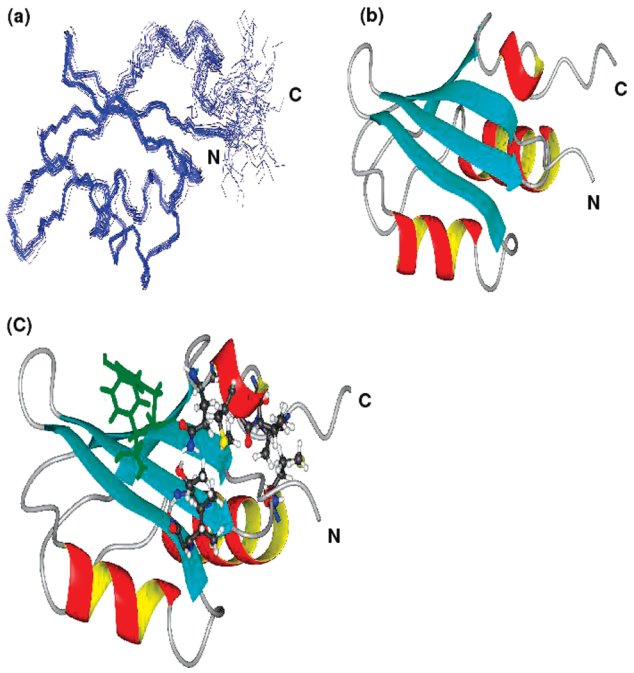

FIGURE 7: Structure of RNA-bound NELF-E RRM. (a) Overlay of the 20 accepted structures, A35−S121, showing the lowest values of the target function. (b) Schematic representation of the lowest energy structure. N- and C-termini are indicated. (c) Residues involved in hydrophobic interactions to stabilize the C-terminus of NELF-E RRM (ball and stick) and the highly conserved aromatic amino acids located in RNP1 and RNP2 (green sticks).

binding by induced fit which is observed in many other RNA binding proteins (*23–26*).

Structural Differences in the C-Terminal Regions of RRMs. The C-terminal extensions of RRM domains are often key in RNA recognition, in several cases forming a helix in the free state that is stabilized by hydrophobic interactions with RNP motifs (*4, 27, 28*). The C-terminal helix of U1A, CstF64, and hnRNP-F RRMs masks the RNA binding β-sheet surface in the absence of the target (Figure 8) (*29*). In U1A RRM the C-terminal helix is repositioned on target binding such that the RNP motifs are accessible for the RNA and, at the same time, the C-terminal helix can also contribute to the specific target RNA hairpin recognition (*20*). Even though the structure of the CstF64 RRM−RNA complex is unknown, it was predicted from NMR relaxation and chemical shift data that the C-terminal helix of CstF64 RRM unfolds upon binding to RNA, rendering the RNP motifs accessible for RNA recognition (*30*). Quasi-RRMs of hnRNP-F, however, recognize RNA without undergoing major conformational changes in the C-terminal helix that also maintains hydrophobic contacts with the RNP motifs (*28*). Thus, the RNA-bound conformations of NELF-E RRM and U1A are very similar even though they are different in the free state (Figure 8).

In conclusion, a wide variety of RNA sequences binds to the NELF-E RRM and induces very similar conformational changes in the protein on binding. While the RNA binding interface is mainly located at the β-sheet surface, rearrangement of residues located in the flexible C-terminal region and the loop between β_3 and α_2 is taking place on binding. Comparison of the free vs the RNA-bound conformation of NELF-E RRM with other RRMs from the known complexes indicates the mechanism of RNA recognition to be unique

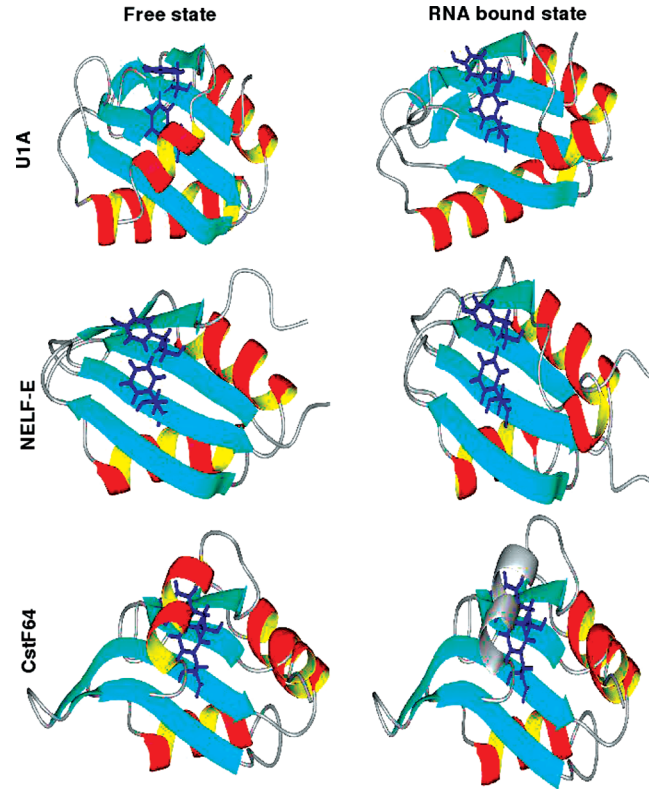

FIGURE 8: Comparison of free and RNA conformations of RRMs. The canonical RNA binding interface is indicated by showing the conserved aromatic amino acids in stick representation. The C-terminal helices are located at the solvent-exposed side of the antiparallel β-sheet surface. The unfolding of the C-terminal helix in the RNA-bound state of CstF64 RRM is represented in gray color. PDB codes for free and RNA-bound RRM are as follows: NELF-E, 2bz2 and 2jx2; U1A, 1fht and 1urn; CstF64, 1p1t.

for NELF-E, but a complete three-dimensional structure of the NELF-E RRM−RNA complex would be needed for the detailed understanding of these differences at the atomic scale.

SUPPORTING INFORMATION AVAILABLE

Structural statistics and determination of K_d values based on chemical shift changes upon RNA titration. This material is available free of charge via the Internet at http://pubs.acs.org.

REFERENCES

1. Bandziulis, R. J., Swanson, M. S., and Dreyfuss, G. (1989) RNA-binding proteins as developmental regulators. *Genes Dev. 3*, 431–437.
2. Kenan, D. J., Query, C. C., and Keene, J. D. (1991) RNA recognition: towards identifying determinants of specificity. *Trends Biochem. Sci. 16*, 214–220.
3. Maris, C., Dominguez, C., and Allain, F. H. (2005) The RNA recognition motif, a plastic RNA-binding platform to regulate post-transcriptional gene expression. *FEBS J. 272*, 2118–2131.
4. Nagai, K., Oubridge, C., Jessen, T. H., Li, J., and Evans, P. R. (1990) Crystal structure of the RNA-binding domain of the U1 small nuclear ribonucleoprotein A. *Nature 348*, 515–520.
5. Allain, F. H., Gubser, C. C., Howe, P. W., Nagai, K., Neuhaus, D., and Varani, G. (1996) Specificity of ribonucleoprotein interaction determined by RNA folding during complex formulation. *Nature 380*, 646–650.
6. Yamaguchi, Y., Takagi, T., Wada, T., Yano, K., Furuya, A., Sugimoto, S., Hasegawa, J., and Handa, H. (1999) NELF, a multisubunit complex containing RD, cooperates with DSIF to repress RNA polymerase II elongation. *Cell 97*, 41–51.

7. Wu, C. H., Yamaguchi, Y., Benjamin, L. R., Horvat-Gordon, M., Washinsky, J., Enerly, E., Larsson, J., Lambertsson, A., Handa, H., and Gilmour, D. (2003) NELF and DSIF cause promoter proximal pausing on the hsp70 promoter in *Drosophila*. *Genes Dev. 17*, 1402–1414.
8. Aida, M., Chen, Y., Nakajima, K., Yamaguchi, Y., Wada, T., and Handa, H. (2006) Transcriptional pausing caused by NELF plays a dual role in regulating immediate-early expression of the junB gene. *Mol. Cell. Biol. 26*, 6094–6104.
9. Ping, Y. H., and Rana, T. M. (2001) DSIF and NELF interact with RNA polymerase II elongation complex and HIV-1 Tat stimulates P-TEFb-mediated phosphorylation of RNA polymerase II and DSIF during transcription elongation. *J. Biol. Chem. 276*, 12951–12958.
10. Fujinaga, K., Irwin, D., Huang, Y., Taube, R., Kurosu, T., and Peterlin, B. M. (2004) Dynamics of human immunodeficiency virus transcription: P-TEFb phosphorylates RD and dissociates negative effectors from the transactivation response element. *Mol. Cell. Biol. 24*, 787–795.
11. Yamaguchi, Y., Inukai, N., Narita, T., Wada, T., and Handa, H. (2002) Evidence that negative elongation factor represses transcription elongation through binding to a DRB sensitivity-inducing factor/RNA polymerase II complex and RNA. *Mol. Cell. Biol. 22*, 2918–2927.
12. Narita, T., Yamaguchi, Y., Yano, K., Sugimoto, S., Chanarat, S., Wada, T., Kim, D. K., Hasegawa, J., Omori, M., Inukai, N., Endoh, M., Yamada, T., and Handa, H. (2003) Human transcription elongation factor NELF: identification of novel subunits and reconstitution of the functionally active complex. *Mol. Cell. Biol. 23*, 1863–1873.
13. Wei, P., Garber, M. E., Fang, S. M., Fischer, W. H., and Jones, K. A. (1998) A novel CDK9-associated C-type cyclin interacts directly with HIV-1 Tat and mediates its high-affinity, loop-specific binding to TAR RNA. *Cell 92*, 451–462.
14. Garber, M. E., Wei, P., KewalRamani, V. N., Mayall, T. P., Herrmann, C. H., Rice, A. P., Littman, D. R., and Jones, K. A. (1998) The interaction between HIV-1 Tat and human cyclin T1 requires zinc and a critical cysteine residue that is not conserved in the murine CycT1 protein. *Genes Dev. 12*, 3512–3527.
15. Peterlin, B. M., and Price, D. H. (2006) Controlling the elongation phase of transcription with P-TEFb. *Mol. Cell 23*, 297–305.
16. Rao, J. N., Neumann, L., Wenzel, S., Schweimer, K., Rosch, P., and Wohrl, B. M. (2006) Structural studies on the RNA-recognition motif of NELF E, a cellular negative transcription elongation factor involved in the regulation of HIV transcription. *Biochem. J. 400*, 449–456.
17. Handa, N., Nureki, O., Kurimoto, K., Kim, I., Sakamoto, H., Shimura, Y., Muto, Y., and Yokoyama, S. (1999) Structural basis for recognition of the tra mRNA precursor by the Sex-lethal protein. *Nature 398*, 579–585.
18. Wang, X., and Tanaka Hall, T. M. (2001) Structural basis for recognition of AU-rich element RNA by the HuD protein. *Nat. Struct. Biol. 8*, 141–145.
19. Ding, J., Hayashi, M. K., Zhang, Y., Manche, L., Krainer, A. R., and Xu, R. M. (1999) Crystal structure of the two-RRM domain of hnRNP A1 (UP1) complexed with single-stranded telomeric DNA. *Genes Dev. 13*, 1102–1115.
20. Allain, F. H., Howe, P. W., Neuhaus, D., and Varani, G. (1997) Structural basis of the RNA-binding specificity of human U1A protein. *EMBO J. 16*, 5764–5772.
21. Volpon, L., D'Orso, I., Young, C. R., Frasch, A. C., and Gehring, K. (2005) NMR structural study of TcUBP1, a single RRM domain protein from *Trypanosoma cruzi*: contribution of a beta hairpin to RNA binding. *Biochemistry 44*, 3708–3717.
22. Fleming, K., Ghuman, J., Yuan, X., Simpson, P., Szendroi, A., Matthews, S., and Curry, S. (2003) Solution structure and RNA interactions of the RNA recognition motif from eukaryotic translation initiation factor 4B. *Biochemistry 42*, 8966–8975.
23. Puglisi, J. D., Chen, L., Blanchard, S., and Frankel, A. D. (1995) Solution structure of a bovine immunodeficiency virus Tat-TAR peptide-RNA complex. *Science 270*, 1200–1203.
24. Faber, C., Scharpf, M., Becker, T., Sticht, H., and Rosch, P. (2001) The structure of the coliphage HK022 Nun protein-lambda-phage boxB RNA complex. Implications for the mechanism of transcription termination. *J. Biol. Chem. 276*, 32064–32070.
25. Battiste, J. L., Mao, H., Rao, N. S., Tan, R., Muhandiram, D. R., Kay, L. E., Frankel, A. D., and Williamson, J. R. (1996) Alpha helix-RNA major groove recognition in an HIV-1 rev peptide-RRE RNA complex. *Science 273*, 1547–1551.
26. Legault, P., Li, J., Mogridge, J., Kay, L. E., and Greenblatt, J. (1998) NMR structure of the bacteriophage lambda N peptide/boxB RNA complex: recognition of a GNRA fold by an arginine-rich motif. *Cell 93*, 289–299.
27. Perez Canadillas, J. M., and Varani, G. (2003) Recognition of GU-rich polyadenylation regulatory elements by human CstF-64 protein. *EMBO J. 22*, 2821–2830.
28. Dominguez, C., and Allain, F. H. (2006) NMR structure of the three quasi RNA recognition motifs (qRRMs) of human hnRNP F and interaction studies with Bcl-x G-tract RNA: a novel mode of RNA recognition. *Nucleic Acids Res. 34*, 3634–3645.
29. Avis, J. M., Allain, F. H., Howe, P. W., Varani, G., Nagai, K., and Neuhaus, D. (1996) Solution structure of the N-terminal RNP domain of U1A protein: the role of C-terminal residues in structure stability and RNA binding. *J. Mol. Biol. 257*, 398–411.
30. Deka, P., Rajan, P. K., Perez-Canadillas, J. M., and Varani, G. (2005) Protein and RNA dynamics play key roles in determining the specific recognition of GU-rich polyadenylation regulatory elements by human Cstf-64 protein. *J. Mol. Biol. 347*, 719–733.
31. Hajduk, P. J., Dinges, J., Miknis, G. F., Merlock, M., Middleton, T., Kempf, D. J., Egan, D. A., Walter, K. A., Robins, T. S., Shuker, S. B., Holzman, T. F., and Fesik, S. W. (1997) NMR-based discovery of lead inhibitors that block DNA binding of the human papillomavirus E2 protein. *J. Med. Chem. 40*, 3144–3150.
32. Johnson, B. A., and Blevins, R. A. (1994) NMRview: A computer program for the visualization and analysis of NMR data. *J. Biomol. NMR 4*, 603–614.
33. Nilges, M., Clore, G. M., and Gronenborn, A. M. (1988) Determination of three-dimensional structures of proteins from interproton distance data by hybrid distance geometry-dynamical simulated annealing calculations. *FEBS Lett. 229*, 317–324.
34. Nilges, M., Clore, G. M., and Gronenborn, A. M. (1988) Determination of three-dimensional structures of proteins from interproton distance data by dynamical simulated annealing from a random array of atoms. Circumventing problems associated with folding. *FEBS Lett. 239*, 129–136.
35. Folmer, R. H., Hilbers, C. W., Konings, R. N., and Nilges, M. (1997) Floating stereospecific assignment revisited: application to an 18 kDa protein and comparison with J-coupling data. *J. Biomol. NMR 9*, 245–258.
36. Ikura, M., Kay, L. E., Tschudin, R., and Bax, A. (1990) Three-dimensional NOESY-HMQC spectroscopy of a ^{13}C-labeled compound. *J. Magn. Reson. 86*, 204–209.
37. Talluri, S., and Wagner, G. (1996) An optimized 3D NOESY-HSQC. *J. Magn. Reson., Ser. B 112*, 200–205.

BI702429M